THE IMPLICIT FINITE DIFFERENCE METHOD IN THE DEFORMATION MECHANICS OF HOMOGENEOUS AND PIECEWISE HOMOGENEOUS BODIES

V. M. Akhundov[*]

The implicit finite difference method for solving deformation problems of mechanics of piecewise-homogeneous bodies is presented. The method is based on approximating the sought-for quantities by polynomials with indeterminate coefficients. It allows one to approximate the derivatives in resolving equations based on a grid with an irregular, in general, arrangement of nodal points. Relations were given for one-, two-, and three-dimensional approximations of the second-order of accuracy. This method was applied to studying the deformation of an elastic rotating cylinder whose matrix is reinforced in the circumferential directions with one layer of round fibers. The material configuration of the cylinder at large displacements and deformations are presented together with the stresses of contact interaction between the matrix and fibers. Its deformation characteristic, which reflects the continuation of the solution of the problem in terms of rotation speed, is determined. The results obtained are compared with the solution of the problem for a cylinder with square fibers at the same filling found by the methods of implicit finite differences and the traditional method of finite differences. Boundary-value problems for a thick-walled cylinder made of an isotropic material are also solved in nonlinear and linear formulations with uniform and nonuniform distributions of nodal points across the cylinder thickness, and the results obtained are compared with the exact solution of the corresponding linear problem.

National Metallurgical Academy of Ukraine, Dnepropetrovsk
[*]Corresponding author; e-mail: akhundov@ua.fm

Formulation of the Problem

Deformation problems of composite bodies are usually solved by modeling their material with the original structure as a homogeneous anisotropic medium with macroscopically equivalent properties. The advantage of the approach based on determining the mechanical characteristics of a body material from the mechanical properties of constituent components is that its implementation requires relatively small computational resources, comparable to those in a numerical study of a homogeneous body. However, on its basis, the internal fields in material components are not directly revealed, and the analysis of their fracture is limited. In addition, the formulas for calculating the effective moduli are based on linear relations of deformation mechanics, which are applicable in the range of rather small deformations. In the case of large deformations, some of the effective moduli are usually used, which are determined from natural experiments with particular types of material deformation. The mechanical characteristics revealed in this case can be used to study a body made of the tested material only with appropriately limited deformations.

Dwelling mainly on the studies of cylindrical bodies with a fibrous structure, we should mention work [1], where a momentless cylindrical shell, unidirectionally reinforced with fibers, is considered employing the effective moduli of its material. In [2, 3], shells of an even number of layers with a crossed arrangement of fibers were studied. The material of each layer is considered for by its effective moduli. The main material of a cylindrical shell reinforced with poorly extensible fibers in the cross-ply pattern was considered as physically nonlinear in [4]. In [5], an artery in the form of a circular two-layer cylindrical tube with large deformations, in which collagen fibers were reinforcing elements, was investigated. The potential law for a nonlinear elastic behavior requires three material constants for each layer in order to take into account the joint reaction of artery wall on the action of axial tension, pressure, and torsion, which were determined from experiments. In [6], the viscoelastic deformation of an artery was also studied by modeling its material as effectively orthotropic.

The most general approach to the study of bodies with a fibrous structure is based on the application of a piecewise homogeneous medium model. In this model, the matrix and fibers are considered as contact-interacting components based on the equations of deformation mechanics with identification of the internal fields of the composite structure. As an example, let us point out the work [7], which presents a study of a metal composite with a copper matrix and tungsten fibers under macroscopically uniform transverse compression. The finite-element method (FEM) is used to calculate internal fields for a limited area of a material with a small number of irregularly spaced fibers during elastoplastic deformation of the components. The finite-element modeling of the deformation processes of fibrous composites at large plastic and creep deformations is described in [8]. In [9], a finite-element model was constructed to characterize the stress-strain state of a unidirectionally reinforced material in tension. In [10], using a grid of plane finite elements, the behavior of an elastoplastic beam reinforced in the transverse direction with elastic fibers of square cross section was investigated. In [11], on the basis of relations of the linear elasticity theory, the problem of edge effects in a layered composite material with isotropic layers of constant thickness under uniaxial loading was solved. An approximate solution of the problem was found by the variational-difference method. In [12], using the finite-element method in a two-dimensional formulation, the compression of a bundle of round fibers between two rigid plates in the cases of small and finite elastic deformations was investigated.

Within the framework of a two-level carcass theory, the model of a piecewise-homogeneous medium for the blocks of representing the material medium [13]. In [14], a problem for the body as a whole was solved by the carcass theory by considering extreme problems according to high-gradient scheme for block assemblies near the boundary surface of the body. With round fibers of reinforcing systems, solutions of micro boundary-value problems for material blocks or their assemblies were found by the method of local variations [15] based on a finite-element approximation [16]. In [17], the problem of large elastic deformations of a multilayer cylinder with circular fibers of square cross section under the action of rotation was solved. The correct shapes of the axial section of the cylinder and the sections of fibers in it made it possible to solve the problem of its deformation by the finite-difference method (FDM). In [18], using the FDM, the behavior of a three-layer pipe reinforced with square fibers and loaded with an internal pressure was investigated.

An important advantage of the FDM in comparison with the FEM in studying of problems based on differential equations is the rather simple formation of numerical analogs of equations of the problem at nodal points of its discrete
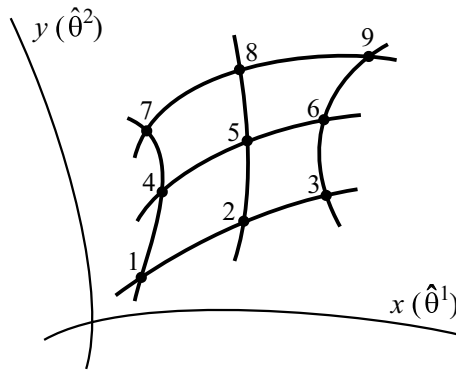
Fig. 1. Configuration of the positions of nine nodal points for approximating the derivative with respect to the coordinates $x \; (\hat{\theta}^1)$ and $y \; (\hat{\theta}^2)$.

scheme. However, this procedure is usually performed using the standard mesh of anchor points, which can be applied to a solid bounded by coordinate surfaces. There are also cases with the use of an uneven arrangement of nodal points near the boundary surface of a body of irregular configuration, when they are located at the intersections of mesh lines with its boundary. The applied formulas for the derivatives at such points are of a special nature (see, for example, [19]). The irregular arrangement of nodal points inside the body and in its boundary surface, which occur in the case of FEM, is not taken into account in the FDM.

An essential factor is the determination of stresses by the FDM with the same accuracy with which displacements are found, when in the boundary-value problem solved these quantities are considered as mutually independent and are determined together on the basis of the system of equations formed. In the FEM, deformations and stresses are determined in the form of displacements using a numerical differentiation with respect to the coordinate variables previously found from the solution of the displacement problem. This operation is the source of significant errors for the quantities indicated, at relatively insignificant errors of the displacements themselves.

In this paper, within the framework of expanding the capabilities of FDM as applied to studies of bodies with a piecewise homogeneous structure, a more general scheme of the method is presented. This scheme assumes an uneven distribution of nodal points of the discrete analog of the body in the problem being solved. The nonuniform distribution of nodal points is taken into account based on polynomial approximations of the sought-for quantities with indeterminate coefficients. The approximation coefficients are calculated in the process of numerical implementation of the problem employing values of the approximated function at the nodal points. The approach applied to the numerical differentiation of one-dimensional functions as a method of indeterminate coefficients, is presented in [20]. It is extended to the computation of partial derivatives in two- and three-dimensional problems and is called the method of implicit finite differences (IFDM). This method can be used to solve various problems of deformation mechanics; it is based on predicting a solution to a problem with its subsequent refinement. This is equally true for both linear and nonlinear problems.

1. Scheme of Implicit Finite Differences (IFD)

Consider a two-dimensional approximation of derivatives with respect to the coordinates x and y (instead of $\hat{\theta}^1$ and $\hat{\theta}^2$). The curvilinear in general coordinates x and y can be rectangular Cartesian coordinates. In the surface of the variables x and y, we select nine compactly located nodal points of a grid for the numerical solution of boundary-value or extremal problems (Fig. 1). These points are located unevenly in increments of coordinates with a transition from one point to another. In the figure, they are connected with each other by curved segments (they can be segments of a coordinate line or a contour for dividing areas of adjacent materials). The nodal points of the discrete scheme, as in the case of using

the FEM, can be located on arbitrary (noncoordinate) curves, whose order is determined by the number of points through which the curves pass.

The approximated function, such as one of components of the displacement vector or stress tensor, will be denoted as u. Based on the values of the function at nodal points 1, ..., 9, the sought-for quantity u in the equations of the problem is approximated by the complete second-order polynomial in both coordinate variables

$$u = a_1 + a_2 x + a_3 y + a_4 xy + a_5 x^2 + a_6 y^2 + a_7 x^2 y + a_8 xy^2 + a_9 x^2 y^2 . \tag{1.1}$$

The corresponding expressions for the first derivatives with respect to the coordinates are

$$\frac{\partial u}{\partial x} = a_2 + a_4 y + 2a_5 x + 2a_7 xy + a_8 y^2 + 2a_9 xy^2 ,$$

$$\frac{\partial u}{\partial y} = a_3 + a_4 x + 2a_6 y + a_7 x^2 + 2a_8 xy + 2a_9 x^2 y . \tag{1.2}$$

Expressions for higher-order derivatives are obvious and are not given here. Let us denote the values of coordinates and nodal points 1, ..., 9 as x_1, y_1, ..., x_9, y_9 and the values of the function at these points — as $u_1, ..., u_9$, respectively. Writing expressions for the function at each nodal points using (1.1), we arrive at a system of linear algebraic equations (SLAE) with respect to the coefficients a_1, ..., a_9:

$$u_1 = a_1 + a_2 x_1 + a_3 y_1 + a_4 x_1 y_1 + ... + a_9 x_1^2 y_1^2 ,$$
$$. \quad . \quad . \quad . \quad . \quad .$$
$$. \quad . \quad . \quad . \quad . \quad . \tag{1.3}$$
$$. \quad . \quad . \quad . \quad . \quad .$$
$$u_9 = a_1 + a_2 x_9 + a_3 y_9 + a_4 x_9 y_9 + ... + a_9 x_9^2 y_9^2 .$$

The solution of this system can be brought, as in the case of the commonly used FDM, to finite formulas for a_i, and the derivatives (1.2), expressed directly in terms of the nodal values of the desired quantity, can be used in the equations of the problem. These coefficients, even at a relatively small number of nodal points in the considered configuration of their location, are found using such cumbersome calculations that this realization of the problem is impractical.

The solution of the system of finite-difference equations of the problem of deformation of a body according to the scheme of implicit coefficients is carried by specifying the initial approximation of the nodal values of the sought-for quantities and its subsequent refinement. We refine the nodal values of the quantities using one of the methods for solving systems of nonlinear equations; as a convenient method, we will employ the discrete Newton method [21]. This method does not require an explicit representation of equations — only the way to calculate the expression of their left-hand sides (to the left of the equal-to-zero sign) has to be known. This method is highly efficient in continuation of the solution with respect to the loading parameters of the body investigated. In the case of a linear problem, the continuation of the solution is not required — even one iteration of the method leads to the desired solution for any initial approximation of nodal values.

SLAE (1.3) is solved using of an algorithm for a computer solution of the problem of deformation of a homogeneous or piecewise homogeneous body. As a result, the approximation coefficients $a_1, ..., a_9$ for the current nodal point are determined in relation to on the values $u_1, ..., u_9$ of the function at the nodes of the inclusive configuration of the points. The linear form of the relation between the quantities indicated is not required (as a feature of the approach considered), therefore, we present them in the general form

$$a_1 = a_1(u_1, u_2, ..., u_9), ..., a_9 = a_9(u_1, u_2, ..., u_9)$$

(recall that, with respect to nodal values of the sought-for functions, the SLAE is not explicitly formed when solving a linear problem).

Having determined a_i, we calculate the required derivatives (1.2) at the nodal point, passing in the course of numerical implementation of the problem from one nodal point to another. These can be derivatives of x and y with respect
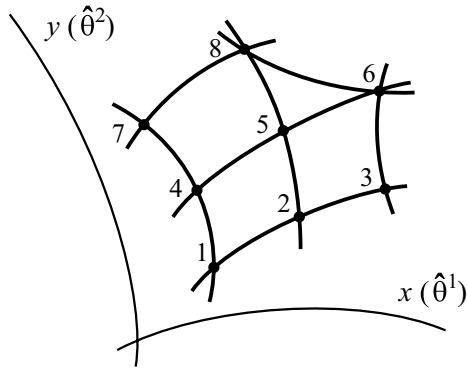
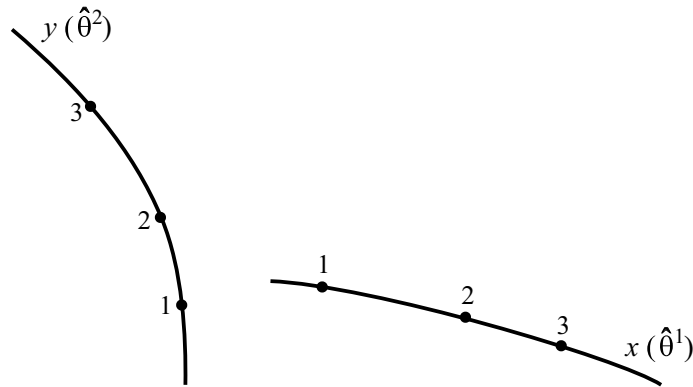Fig. 2. The same on the basis of eight anchor points.

Fig. 3. Configuration of the positions of three nodal points located on each coordinate lines.

to point 5, which is central in the configuration of the location of points 1, ..., 9. For other points, the derivatives are determined on the basis of their adjacent configurations (sets) for which the nodal points are central. In the case of finding derivatives at points located in the boundary surface of a body or at the interface of its constituent components, the same configuration of nodal points employed to calculate the central derivatives are used.

As another set of nodal points for approximating the derivatives, Fig. 2 shows a configuration of eight irregularly spaced anchor points. The relative positions of the points may differ from the given ones, but this will not affect the shape of the applied approximation. Figure 3 shows two configurations with three nodal points, each of them located on the coordinate lines x and y.

In the case of a configuration with eight points, for the function and its derivatives, we employ the approximations

$$u = a_1 + a_2 x + a_3 y + a_4 xy + a_5 x^2 + a_6 y^2 + a_7 x^2 y + a_8 xy^2 ; \tag{1.4}$$

$$\frac{\partial u}{\partial x} = a_2 + a_4 y + 2a_5 x + 2a_7 xy + a_8 y^2 ,$$

$$\frac{\partial u}{\partial y} = a_3 + a_4 x + 2a_6 y + a_7 x^2 + 2a_8 xy , \tag{1.5}$$

in the case of a configuration with three points located along the x-coordinate line — the approximations

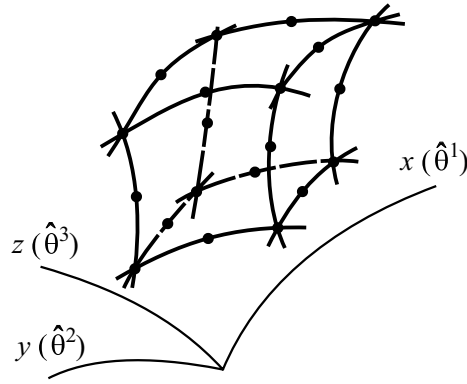$$u = a_1 + a_2 x + a_3 x^2 ; \quad \frac{\partial u}{\partial x} = a_2 + 2a_3 x , \tag{1.6}$$

Fig. 4. Configuration of the positions of 20 nodal points for approximating derivatives with respect to the coordinates $x\,(\bar\theta^1)$, $y\,(\bar\theta^2)$, and $z\,(\bar\theta^3)$.

and for points located along the y-coordinate line —

$$u = a_1 + a_2 y + a_3 y^2 \; ; \quad \frac{\partial u}{\partial y} = a_2 + 2a_3 y \; . \tag{1.7}$$

Due to their obviousness, we do not present the corresponding SLAEs for determining the coefficients a_i in (1.4) - (1.7) in terms of the values u_i of the function at the nodal points (x_i, y_i).

When three nodal points are located on a coordinate line at equal distances h between them as increments of the coordinate when passing from one point to another adjacent to it, the calculations based on approximations (1.6), (1.7) are greatly simplified. In these cases, we arrive at the well-known formulas [19] for the right, central, and left derivatives with respect to the coordinate at these points in accordance with their location on the line. Thus, if points 1, 2, and 3 are located on the x-line and are separated by equal coordinate distances h, then, for the derivatives with respect x to these points, we find that

$$\frac{\partial u}{\partial x}\bigg|_1 = \frac{-3u_1 + 4u_2 - u_3}{2h} \; , \quad \frac{\partial u}{\partial x}\bigg|_2 = \frac{u_3 - u_1}{2h} \; , \quad \frac{\partial u}{\partial x}\bigg|_3 = \frac{u_1 - 4u_2 + 3u_3}{2h} \; . \tag{1.8}$$

As in two-dimensional approximations (1.1), (1.2) and (1.4), (1.5), one-dimensional (1.6) and (1.7), a three-dimensional approximation of quantities and their derivatives is constructed on the basis, in the general case, of a system of curvilinear spatial coordinates x, y, z. In its most complete form, the second-order approximation is based on the use of 27 nodal points. The positions of these points determine the configuration of an oblique hexagon with curved edges and the location of eight points at its vertices — six on the edges, 12 on the edges, and one inside the body. The corresponding representations of the function being approximated and its derivatives are written as

$$u = \sum_{i,j,k=0}^{2} a_{ijk} x^i y^j z^k \; ; \tag{1.9}$$

$$\frac{\partial u}{\partial x} = \sum_{j,k=0,i=1}^{2} i a_{ijk} x^{i-1} y^j z^k \; , \quad \frac{\partial u}{\partial y} = \sum_{i,k=0,j=1}^{2} j a_{ijk} x^i y^{j-1} z^k \; ,$$

$$\frac{\partial u}{\partial z} = \sum_{i,j=0,k=1}^{2} k a_{ijk} x^i y^j z^{k-1} \; . \tag{1.10}$$

Approximation polynomials can also be used in the absence of anchor points on the faces and inside the hexagon of the configuration of their location. Figure 4 shows a second-order configuration of 20 nodal points, eight of which are
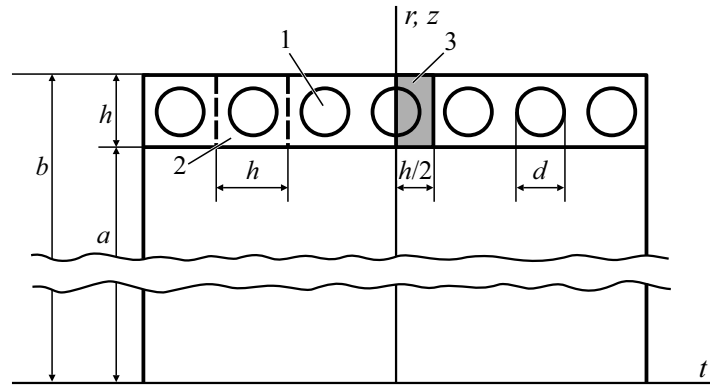
800

Fig. 5. Axial section of a cylindrical body in the initial state: 1 — round fiber; 2 — ring element;
3 — half of the annular element to the right of the central section.

located at vertices of the configuration, and the remaining 12 — on its contour edges. The approximation of the function for a given set of nodal points is presented in the expanded form

$$u = a_1 + a_2 x + a_3 y + a_4 z + a_5 xy + a_6 yz + a_7 xz + a_8 x^2 + a_9 y^2 + a_{10} z^2$$

$$+ a_{11} xyz + a_{12} xy^2 + a_{13} xz^2 + a_{14} yz^2 + a_{15} x^2 y + a_{16} x^2 z + a_{17} y^2 z$$

$$+ a_{18} x^2 yz + a_{19} y^2 xz + a_{20} z^2 xy, \tag{1.11}$$

and the corresponding derivatives are obvious. Polynomial (1.11) contains the products of powers of coordinate variables $x^i y^j z^k$, which are included as form functions of a second-order three-dimensional finite element from a serendip family [3].

In the IFDM, the derivatives based on the applied configuration of nodal points, in contrast to the FEM, are usually calculated for the central one. With transition to another nodal point, a different set of nodal points is used, including its set, as is the case in the applied finite-difference method with determinate coefficients. As in the case of FDM, this order is violated on the boundary surface of the body and on interfaces of dissimilar materials in it. The approach is simple enough to be algorithmized and can be extended to higher-order approximations.

At the same time, the implicit scheme of the finite-element method can also be used. This version of the finite-element method is based on the implicit calculation of displacement approximation coefficients (1.9) and their derivatives (1.10). The approximation is performed based on the same set of node points of a finite element, but calculations are performed for the region of given FE, in accordance with the piecewise smoothness of the function being approximated.

The laborious procedure for formation of the stiffness matrix of the body (structure) is not required. Moreover, its implementation is possible only on the basis of a linear or linearized formulation of the problem. In the case of an implicit FEM scheme, at the nodal points common to adjacent FEMs, the equations themselves are summed up directly related to the variations in displacements of these points. This procedure is simpler than the formation of the stiffness matrix; it can be applied to both linear and geometrically and physically nonlinear problems. The resulting equations of the method are solved for nodal displacements by the direct implementation of the numerical integration in the equations. The integration is performed for each finite element based on the next approximation of the values of its nodal displacements. As a method that refines the approximation of nodal displacements, one can use the discrete Newton method or one of the optimization methods [22] with continuation along the loading history.

2. Conditions for Setting the Problem

The diagram of a single-layer circular cylinder with circular fibers located in it along the circumferential direction is shown in Fig. 5. The cylindrical body was modeled as an assembly of annular elements along the horizontal direction

(generatrix). The annular element was a $h \times h$ square elastomeric ring having a circular fiber with a diameter d made of a stiffer elastomer than its core. The inner radius is $r = a$ of the cylinder and the outer one is $r = a + h = b$.

We investigated the axisymmetric deformation of the cylinder under the action of rotational motion in deformation conditions when displacements in the boundary surfaces of the annular elements transverse to the cylinder axis take place in the planes of their initial arrangement. Due to symmetry, the problem was solved for the right half of the annular element enclosed between the cross sections of the cylinder one of which passes through the axial line of the fiber of the annular element ($t = 0$) and the other — through the matrix in the middle between the axial lines of two fibers in adjacent annular elements ($t = h / 2$).

The material cylindrical coordinates $\hat{\theta}^1, \hat{\theta}^2, \hat{\theta}^3$, were used, which were designated as t, φ, r in the reference configuration of the cylindrical body (axial, circumferential and radial coordinates, respectively). The axial coordinate t was measured from the cross section of the cylinder in which the axial line of the fiber of the annular element was located. Along with the radial coordinate r, the coordinate $z = r - a$ measured from the inner surface of the cylinder with radius a was used. The physical components of vector and tensor quantities were indicated by coordinate indices enclosed in parentheses. The values related to the matrix and fibers were marked with an index n; with $n = 0$ corresponds to the matrix and $n = 1$ — to the fiber. The indices m and f, respectively, were also used.

3. Equations of the Mathematical Model

We proceeded from the kinematic equations of nonlinear mechanics that determine the components of the Cauchy–Green strain measure [23]. For components of this tensor under axisymmetric deformation of the matrix and fiber in the circular element of the cylinder, we arrive at the following expressions:

$$g_{n(11)} = \lambda_{n1}^2 = \left(1 + \frac{\partial u_{n(1)}}{\partial t}\right)^2 + \left(\frac{\partial u_{n(3)}}{\partial t}\right)^2,$$

$$g_{n(22)} = \lambda_{n2}^2 = \left(1 + \frac{u_{n(3)}}{r}\right)^2,$$

(3.1)

$$g_{n(33)} = \lambda_{n3}^2 = \left(1 + \frac{\partial u_{n(3)}}{\partial r}\right)^2 + \left(\frac{\partial u_{n(1)}}{\partial r}\right)^2,$$

$$g_{n(13)} = \lambda_{n1}\lambda_{n3} \cos \omega_{n13} = \frac{\partial u_{n(1)}}{\partial r} + \frac{\partial u_{n(3)}}{\partial t} + \frac{\partial u_{n(1)}}{\partial t} \cdot \frac{\partial u_{n(1)}}{\partial r} + \frac{\partial u_{n(3)}}{\partial t} \cdot \frac{\partial u_{n(3)}}{\partial r}$$

$$n = 0,1$$

(the components of vector and tensor quantities equal to zero under the symmetry conditions of the problem being solved are not given), where λ_{n1}, λ_{n2}, and λ_{n3} are the stretch ratios in directions of the coordinate lines $\hat{\theta}^1$, $\hat{\theta}^2$, $\hat{\theta}^3$ (t, φ, r) respectively; ω_{n13} is the angle between the $\hat{\theta}^1$- and $\hat{\theta}^3$-coordinate lines.

In the case of a compressible matrix and fiber materials, the components of the symmetric Piola–Kirchhoff stress tensors are related to the components of strain tensors by the relations

$$J_n \sigma_{n(ij)} = 2 \sum_{p=1}^{q} \frac{\partial W_n}{\partial I_p} \cdot \frac{\partial I_p}{\partial g_{n(ij)}}, \quad i, j = 1, \ldots, 3, \quad n = 0,1 \quad (J_n = | g_{n(ij)} |^{1/2}),$$

(3.2)

where $W_n = W_n[I_1(g_{n(ij)}), I_2(g_{n(ij)}),..., I_q(g_{n(ij)})]$ is the elastic potential of the matrix material ($n = 0$) or fiber ($n = 1$), determined as a function of invariants $I_1, I_2,..., I_q$ of its deformation tensor; J_n is the multiplicity factor of changes in the local volume of the material component.

At large (finite) deformations, the equilibrium equations lead to the following equilibrium equations for the binder and fiber at axisymmetric deformation in the metric of the reference configuration:

$$\frac{\partial t_{n(11)}}{\partial t} r + \frac{\partial t_{n(31)}}{\partial r} r + t_{n(31)} = 0 \,,$$

$$\frac{\partial t_{n(13)}}{\partial t} r + \frac{\partial t_{n(33)}}{\partial r} r + t_{n(33)} - t_{n(22)} + \rho_n r F_{n(3)} = 0 \,, \tag{3.3}$$

$$n = 0,1\,.$$

Here, $t_{n(ij)}$ are the physical components of the asymmetric Piola stress tensor for the matrix and fiber, whose non-zero components are determined by the expressions

$$t_{n(11)} = J_n \sigma_{n(11)} \left(1 + \frac{\partial u_{n(1)}}{\partial t} \right) + J_n \sigma_{n(13)} \frac{\partial u_{n(1)}}{\partial r} \,,$$

$$t_{n(13)} = J_n \sigma_{n(13)} \left(1 + \frac{\partial u_{n(3)}}{\partial r} \right) + J_n \sigma_{n(11)} \frac{\partial u_{n(3)}}{\partial t} \,,$$

$$t_{n(31)} = J_n \sigma_{n(31)} \left(1 + \frac{\partial u_{n(1)}}{\partial t} \right) + J_n \sigma_{n(33)} \frac{\partial u_{n(1)}}{\partial r} \,, \tag{3.4}$$

$$t_{n(33)} = J_n \sigma_{n(33)} \left(1 + \frac{\partial u_{n(3)}}{\partial r} \right) + J_n \sigma_{n(31)} \frac{\partial u_{n(3)}}{\partial t} \,,$$

$$t_{n(22)} = J_n \sigma_{n(22)} \left(1 + \frac{u_{n(3)}}{r} \right) . \tag{3.5}$$

When the distance from material points of the cylinder to its axis changes under the influence of rotation, the radial component of the density of body forces in the second of equation (3.3) is

$$F_{n(3)} = (r + u_{n(3)})\omega^2 \,, \quad n = 0,1 \,,$$

where $\omega = 2\pi f$ is the angular speed of rotation and f is the number of revolutions per second.

The components $J\sigma_{(ij)}$ of the Piola–Kirchhoff symmetric stress tensor are expressed in terms of components p_{ij} of the stress vectors on the θ^i-coordinate surfaces. They are referred to the normalized vector basis of the coordinate system in the deformed cylinder configuration according to the formulas [24]

$$J\sigma_{(11)} = \lambda_1^{-1}\lambda_2\lambda_3 \sin \omega_{23} p_{11} \,, \quad J\sigma_{(22)} = \lambda_2^{-1}\lambda_1\lambda_3 \sin \omega_{13} p_{22} \,,$$

$$J\sigma_{(33)} = \lambda_3^{-1}\lambda_1\lambda_2 \sin \omega_{12} p_{33} \,, \quad J\sigma_{(13)} = \lambda_2 \sin \omega_{23} p_{13} \,, \tag{3.6}$$

$$J\sigma_{(31)} = \lambda_2 \sin \omega_{12} p_{31} \quad (= J\sigma_{(13)})$$

(the subscript "n" indicating to the matrix or fiber is omitted).

4. Formulation of the Boundary-Value Problem and its Numerical Solution

The geometric (3.1), physical (governing) (3.2), and equilibrium (3.3) equations, together with (3.4) and (3.5), are the resolving equations of the boundary-value problem for a piecewise homogeneous cylinder. The components $u_{n(1)}$ and $u_{n(3)}$ of displacement vectors and the components $t_{n(11)}$, $t_{n(13)}$, $t_{n(31)}$, and $t_{n(33)}$ of the stress tensors in the matrix and fibers were taken as basic quantities. The components $g_{n(11)}$, $g_{n(22)}$, $g_{n(33)}$, $g_{n(13)}$ of the strain measure tensor and the component $t_{n(22)}$ of the stress tensor appearing in the resolving equations were expressed in terms of the basic quantities using (3.1), (3.2), and (3.5).

The boundary conditions for the binder and fibers of the cylinder at which the boundary value problem was solved, express the absence of axial displacements in the surfaces $t = 0$ and $t = h/2$ and transverse displacements from these surfaces:

$$u_{n(1)}\big|_{t=0} = 0, \quad g_{n(13)}\big|_{t=0} = 0, \quad u_{n(1)}\big|_{t=h/2} = 0, \quad g_{n(13)}\big|_{t=h/2} = 0, \qquad (4.1)$$

$$n = 0,1.$$

With internal and external surfaces $r = a$ and $r = b$ free from loads, the conditions in them are reduced to the trivial form

$$t_{m(31)}\big|_{r=a} = 0, \quad t_{m(33)}\big|_{r=a} = 0, \qquad (4.2)$$

$$t_{m(31)}\big|_{r=b} = 0, \quad t_{m(33)}\big|_{r=b} = 0,$$

where the subscript m indicates the quantities in the boundary surfaces as referring to the matrix (binder).

The conditions of joint deformation were set by the equalities of the components of the vectors of displacements and stresses for the matrix and the fiber within boundaries of their separation:

$$u_{m(1)}(t,r) = u_{f(1)}(t,r), \quad u_{m(3)}(t,r) = u_{f(3)}(t,r); \qquad (4.3)$$

$$t_{m(11)}(t,r)\mathring{n}_1 + t_{m(31)}(t,r)\mathring{n}_3 = t_{f(11)}(t,r)\mathring{n}_1 + t_{f(31)}(t,r)\mathring{n}_3,$$

$$\qquad (4.4)$$

$$t_{m(13)}(t,r)\mathring{n}_1 + t_{m(33)}(t,r)\mathring{n}_3 = t_{f(13)}(t,r)\mathring{n}_1 + t_{f(33)}(t,r)\mathring{n}_3,$$

$$(t,r) \in A_{mf},$$

where $\mathring{n}_1$ and $\mathring{n}_3$ are the components of the orientation vector of the surface (contour) A_{mf} of the interface between the matrix and fiber in the undeformed state.

The first-order derivatives of the fundamental quantities with respect to the axial and radial coordinates t and r were approximated using finite-difference relations of the second order of accuracy according to the scheme of implicit coefficients (1.2), (1.5) or (1.6), (1.7) depending on positioning of the nodal points.

For each of the internal points of the finite-difference mesh of nodal points in the cross section of the annular element, difference analogs of two equilibrium equations (3.3) and four physical equations (3.4) were formed. Equations (3.4) in a discrete form were formed using the constitutive (3.2) and deformation (3.1) relations. At the points of boundary surfaces of the annular element, using (3.1), we composed finite-difference analogs of the two corresponding boundary conditions from (4.1) and (4.2) and four physical equations (3.4).

If a nodal point belonged to the interface between the constituent components A_{mf}, it was considered as doubled. One of the doubled points was considered as belonging to the matrix and the other — to the fiber. On one side of the interface between the components of the material, we formed two continuity equations for displacements (4.3) and physical equations (3.4) for the material in it; on the other — two continuity equations for stresses (4.4) together with physical equations for the material in the same side (3.4). Thus, in total, we composed six equations for each of the aligned nodal points, and all other nodal points in the section of the annular element.

A feature of the applied scheme for the numerical solution of the problem is the formation of finite-difference analogs of equilibrium equations only at the internal points of the regions occupied in the body by individual components (matrix and fibers) of the material. The numerical analogs of physical equations were formed at all nodal points of the discrete scheme of the problem: at internal points, points in the outer boundary surface of the body, and at the interfaces of phase materials.

The generated system of nonlinear equations for the basic quantities at the nodal points of the two-dimensional region $a \leq r \leq a+h$, $0 \leq t \leq h/2$ was solved by the discrete Newton method. A stable realization of the boundary-value problem was ensured by continuation of the solution in terms of the angular speed of rotation of the cylinder. As a result of solving the boundary-value problem at a given final speed of rotation with involvement of (3.6), the nodal values of the components of the displacement vector $u_{n(i)}$ and the tensor of stresses $t_{n(ij)}$, strains λ_{ni}, ω_{nij}, and stresses p_{nij} for the matrix ($n=0$) and fiber ($n=1$) were determined.

Components of the stress vector at the interface between the matrix and the fiber relative to the coordinate system in the initial state, referred to the unit of the deformed area, were calculated by the formulas

$$\sigma_{(1)} = (\mathring{n}_{(1)} t_{(11)} + \mathring{n}_{(3)} t_{(31)})(dA/d\mathring{A})^{-1},$$

$$\sigma_{(3)} = (\mathring{n}_{(1)} t_{(13)} + \mathring{n}_{(3)} t_{(33)}) (dA/d\mathring{A})^{-1},$$

$$dA/d\mathring{A} = J(g^{(ij)} \mathring{n}_{(i)} \mathring{n}_{(j)})^{1/2}, \quad i,j = 1,3$$

(we have omitted the index indicating the material component for the quantities used here), where $\mathring{n}_{(1)}$ and $\mathring{n}_{(3)}$ are non-zero components of the unit vector of the outer normal of the interface between the fiber and matrix in the undeformed state; $dA/d\mathring{A}$ is the multiplicity factor of local change in the area of the interface between the components as a result of deformation; J is the multiplicity factor of local changes in the volume of material on one or the other side of the section; $g^{(ij)}$ are the components of the tensor inverse of the Cauchy–Green strain tensor.

The normal σ_n and shear τ_n stresses of contact interaction were found as

$$\sigma_n = \sigma_{(1)}n_{(1)} + \sigma_{(3)}n_{(3)}, \quad \tau_n = -\sigma_{(1)}n_{(3)} + \sigma_{(3)}n_{(1)}$$

(the tensile stress σ_n and counterclockwise shear stress τ_n on the fiber side are positive). Here, $n_{(1)}$ and $n_{(3)}$ are nonzero components of the orientation vector $\boldsymbol{n} = n_{(i)} \mathring{\boldsymbol{r}}_i = n_m \boldsymbol{r}^m$, $i,m = 1,3$ of the deformed interface with respect to the system of cylindrical coordinates in the initial configuration; $\mathring{\boldsymbol{r}}_1$ and $\mathring{\boldsymbol{r}}_3$ are the basis vectors with axial and radial directions, unit length, and orthogonal to each other in the coordinates used. The components $n_{(1)}$ and $n_{(3)}$ of the orientation of the interface in the deformed state were determined through the components n_1 and n_3 of this vector in the deformed coordinate basis by the formula

$$n_{(i)} = n_m g^{(mk)} \left(\delta_k^i + \frac{\partial u_{(i)}}{\partial \widehat{\theta}^k} \right), \quad i, m, k = 1, 3 \quad (\widehat{\theta}^1 = t, \ \widehat{\theta}^3 = r). \tag{4.5}$$

Formulas for the relation between the components of orientation vectors of deformed and undeformed surfaces, in turn, have the form [23]

$$n_m = \left(g^{(jl)} \mathring{n}_{(j)} \mathring{n}_{(l)} \right)^{-1/2} \mathring{n}_{(m)}, \quad m, j, l = 1, 3. \tag{4.6}$$

Relations (4.5) were obtained using the relationship between the mutual and main vectors of the deformed basis, $\boldsymbol{r}^m = g^{(mk)} \boldsymbol{r}_k$, $k,m = 1,3$, and the relationship between the vectors of the deformed and original basis, $\boldsymbol{r}_k = (\delta_k^i + \partial u_{(i)} / \partial \widehat{\theta}^k) \mathring{\boldsymbol{r}}_i$, $i,k = 1,3$. The quantities $n_{(i)}$ and n_m were determined by calculating the one-sided derivatives in (4.5) and (4.6) with respect to the coordinate variables t $(\widehat{\theta}^1)$ and r $(\widehat{\theta}^3)$ from the contact surface.
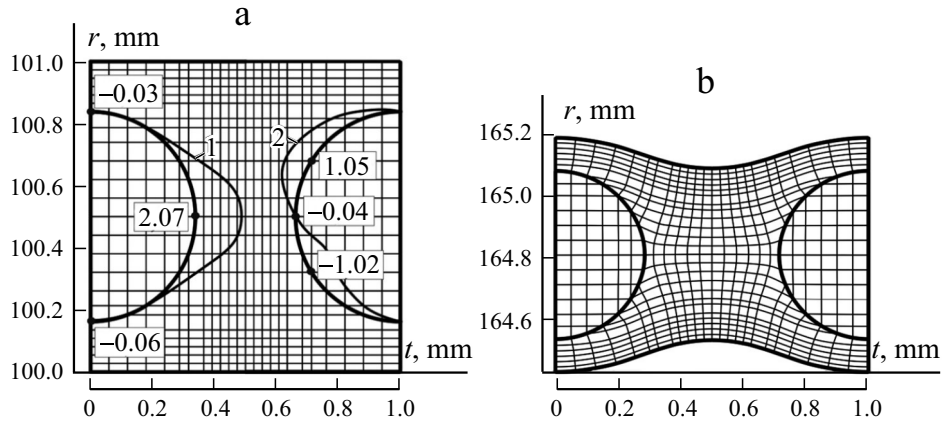
Fig. 6. Initial (a) and deformed (b) at $\omega = 2\pi \cdot 130\,\text{s}^{-1}$ configurations of the axial section of an annular element of a cylinder with circular fibers: 1 and 2 — distributions of normal σ_n and τ_n tangential stresses, respectively, on the left and right halves of the matrix-fiber interface; for characteristic points on the left half of the contour, the values of σ_n are indicated and on the right half of the contour — the values of τ_n.

5. Results of Numerical Research

Results of a numerical study were presented for a thin-walled cylinder with an inner radius $a = 100$ mm, wall thickness $h = 1$ mm, and outer radius $b = a + h = 101$ mm (see Fig. 5). The diameter of fibers was $d_f = \sqrt{4 \cdot 0.36 / \pi} = 0.677$ mm. The distance between the axial lines of adjacent fibers was equal to the cylinder wall thickness $h = 1$ mm. The reinforcement coefficient of the cylinder was $k_f = \pi d^2 / 4 / h^2 = 0.36$, and the densities of matrix and fiber materials were $\rho_m = \rho_f = 1.1 \cdot 10^3$ kg/m³. The physical equations for the matrix material were constructed using the Levinson–Bourges potential [4]

$$W_m = \frac{E_m}{4(1+v_m)} \left[\beta_m \, (I_1 - 3) + (1 - \beta_m)(I_2 I_3^{-1} - 3) \right.$$

$$\left. + 2(1 - 2\beta_m)(\sqrt{I_3} - 1) + \left(2\beta_m + \frac{4v_m - 1}{1 - 2v_m} \right)\left(\sqrt{I_3} - 1 \right)^2 \right] , \tag{5.1}$$

where I_1, I_2, and I_3, are the invariants of the tensor of Cauchy–Lagrange deformation measure. The parameters E_m and v_m characterize the stiffness and compressibility of the material, and β_m is an additional material constant. The elastic modulus of the binder, we took $E_m = 4$ MPa, the compressibility parameter $v_m = 0.46$, and the parameter β_m was assumed equal to one. The behavior of the fiber material was described by the Blitez potential [4]

$$W_f = \frac{E_f}{4(1+v_f)} \left[(I_1 - 3) - \frac{2}{1 - 2v_f} \ln \sqrt{I_3} + \frac{4v_f}{1 - 2v_f}(\sqrt{I_3} - 1) \right]$$

with elasticity modulus $E_f = 68$ MPa and a compressibility parameter $v_f = 0.40$.

Results were obtained using a 25×25 grid of nodal points for the entire cross section of the annular element, counting two aligned points on the matrix-fiber interface as one.

In Fig. 6, material configurations of the cross section of a complete annular element enclosed between the sections $t = 0$ and $t = h$ of the cylinder, in the initial and deformed at $\omega = 2\pi \cdot 130\,\text{s}^{-1}$ states are depicted. The coordinate lines and the contour of fiber section were constructed using cubic interpolation splines. The limiting surfaces of a cylindrical body
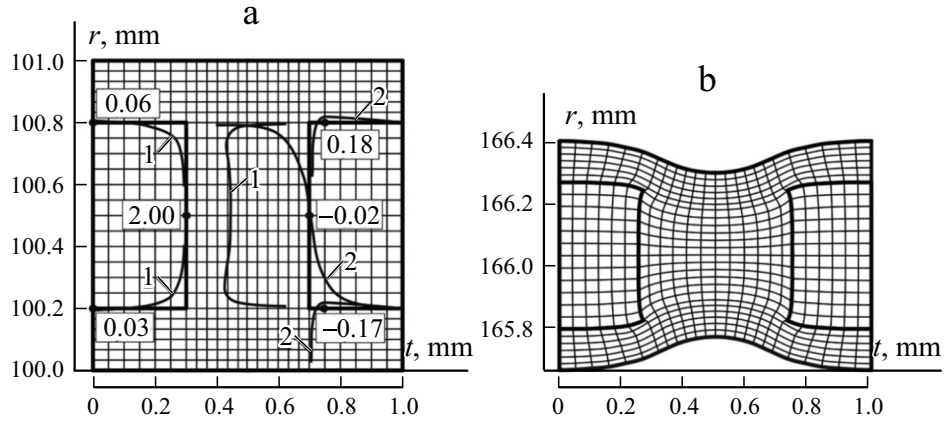
Fig. 7. The same for the annular element of the cylinder with square fibers.

under the influence of rotation acquired a wavy shape (corrugated) with a period along the generatrix equal to the period h of reinforcement. The arrows of waveform deflections (double amplitudes) in the inner and outer surfaces of the shell, defined as

$$f_a = |\, u_{(3)} \,|_{t=0,r=a} \, - u_{(3)} \,|_{t=h/2,r=a} \,|,$$

$$f_b = |\, u_{(3)} \,|_{t=0,r=b} \, - u_{(3)} \,|_{t=h/2,r=b} \,|,$$

differed insignificantly from each other. At the specified rotation speeds $f_a = 0.102$ mm, $f_b = 0.098$ mm, the difference was 4%. The median surface $z = h/2$ $(r = a + h/2)$ in the deformed body remained practically cylindrical. In general, the material configuration of the cylindrical body in the deformed state was close to a cylindrically symmetric relative to the surface $r = a + h/2$ due to the thin wall of the body.

The cross-sectional area of the annular element transverse to its axial line and the cross section of fiber in the achieved state became 1.5 times smaller than in the initial state. In general, the volume occupied by the cylinder material increased by 8% compared with that in the initial state, which was the result of compressibility of the matrix and fiber materials. The cross section of fibers in the deformed state became slightly ellipsoidal, with the ratio between the axes of section with orientations along the t - and r -directions equal to 1.06. This change in geometry during deformation can be explained by the slight elongation and shortening in t - and r -directions in the cross section of the fiber under the influence of a soft matrix.

Calculations were also carried out for cylinders reinforced with square fibers by using the method of IFD. The results coincided with the results of calculations of these cylinders by the method of finite differences — due to the degeneration of formulas (1.2) or (1.5) into FDM formulas (1.8) with determinate coefficients for the derivatives with respect to the corresponding coordinates t and r .

Figure 7 shows the initial configuration and the configuration deformed at $\omega = 2\pi \cdot 130\,\mathrm{s}^{-1}$ of an annular element of the cylinder with fibers of a $\delta \times \delta = 0.6 \times 0.6$ mm square cross section (the cross-sectional area was the same as that of round fibers at the same filling $k_f = 0.36$). The rest of geometrical and physical parameters of the cylinder were the same as in the case with round fibers. We should point to slightly greater wave amplitudes on the inner and outer surfaces at $f_a = 0.106$ mm and $f_b = 0.103$ mm. In this case, in the deformed state, the cross-sectional areas of the annular element and fibers in it were practically the same as in the cylinder with round fibers.

Together with images of undeformed configurations of ring elements with round and square fibers (Figs. 6a and 7a), graphs of the distribution of normal σ_n and tangential τ_n stresses on the interface between the fiber and the matrix from the fiber side were also presented. The curves were obtained by plotting the values of corresponding stresses on the normals
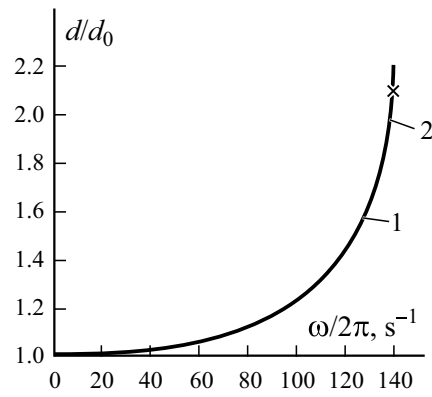
Fig. 8. The multiplicity factor of changes in the diameters of cylinders with fibers of round (1) and square (2) sections at the rotation speed $\omega / 2\pi$; "×" is the end point of the curve for a cylinder with round fibers.

TABLE 1. Displacement Values of the Inner and Outer Surfaces of Cylinders with Round (Numerator) and Square (Denominator) Fibers

$\omega/2\pi$	20	40	100	120	130	135	140
$u_{(3)}\mid_{t=0,\,z=0}$, mm	$\dfrac{0,6271}{0,6208}$	$\dfrac{2,6052}{2,5790}$	$\dfrac{22,915}{22,743}$	$\dfrac{43,582}{43,664}$	$\dfrac{64,431}{65,663}$	$\dfrac{81,984}{85,424}$	$\dfrac{110,78}{122,79}$
Difference, %	1.00	1.01	0.75	−0.19	−1.91	−4.20	−10.8
$u_{(3)}\mid_{t=0,\,z=h}$, mm	$\dfrac{0,6235}{0,6171}$	$\dfrac{2,5905}{2,5641}$	$\dfrac{22,802}{22,628}$	$\dfrac{43,391}{43,468}$	$\dfrac{64,180}{65,401}$	$\dfrac{81,690}{85,114}$	$\dfrac{110,43}{122,40}$
Difference, %	1.03	1.02	0.76	−0.18	−1.90	−4.19	−10.8

to the dividing contours. The normal stress σ_n was plotted at the interface for the left half of fiber and shear stress τ_n — at the interface for its right half.

Note the low compression stresses on the surface of the round fiber and the tensile stress on the surface of the square fiber in rather narrow neighborhoods of the central section $t = 0$ compared with tensile stresses on the surfaces of the fibers in the vicinity of their middle circles $t = d / 2$, $z = h / 2$ and $t = \delta / 2$, $z = h / 2$. The tensile stresses on these circles were close: $\sigma = 2.07$ and 2.00 MPa for round and square fibers, respectively. The results in the case of fibers with a square cross section at its corner points (circumferential lines) are formal due to their special (irregular) nature [25]. With increasing degree of sampling, stresses at these points increased considerably, but the neighborhoods of these points decreased greatly. Therefore, when approaching these points, we cut off the stress curves.

Figure 8 shows the multiplicity factor of changes in the diametrical dimensions d / d_0 of cylindrical bodies with fibers of circular and square sections as a function of the angular speed of rotation ω. In this relation, $d_0 = 2b$ and $d = d_0 + 2u_b$ are diameters of the cylinder in the initial and deformed states; $u_b = u_{(3)}\mid_{t=0,z=h}$ is movement in the radial direction of points on the outer surface of the cylinder at the section $t = 0$. Both curves coincided within the error of their graphical representation at the specified interval of rotation speed. An exception was a small vicinity of the value of $\omega = 2\pi \cdot 140\,\mathrm{s}^{-1}$, which was close to the limiting value of the rotational speed at which the diameter of a cylinder with square fibers was noticeably greater than with round fibers.

Table 1 shows the radial displacements $u_{(3)}\mid_{t=0,\,z=0}$ and $u_{(3)}\mid_{t=0,\,z=h}$ of the inner and outer surfaces of cylinders with fibers of round and square sections at different speeds of rotation. In the range of $0 \le \omega / 2\pi \le 115\,\mathrm{s}^{-1}$, the values $u_{(3)}$ of a cylinder with round fibers slightly exceed the corresponding displacements of a cylinder with square fiber. The dif-
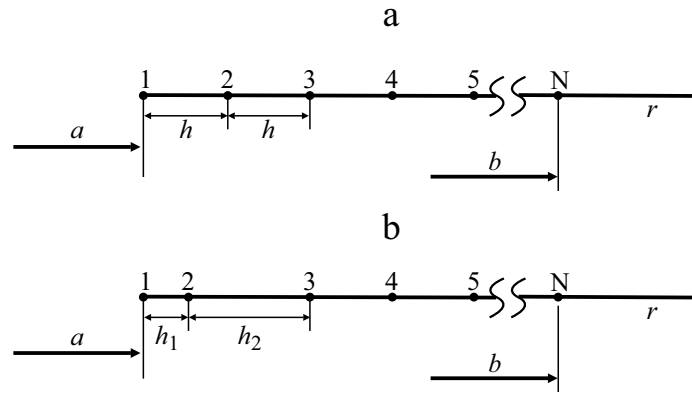
a

b

Fig. 9. Uniform (a) and nonuniform (b) arrangements of nodal points along the radial coordinate for an isotropic cylinder: $a = 100$ mm, $b = 200$ mm; N — total number of odd nodal points; $h_1 + h_2 = 2h$.

TABLE 2. Displacements of the Inner Surface of an Isotropic Cylinder ($a = 100$ Mm, $b = 200$ Mm) at $\omega = 2\pi \cdot 10\,\mathrm{s}^{-1}$ From Solutions of the Boundary-Value Problem in the Linear Formulation

N	First-order approximation		Second-order approximation	
	$h_1 = h_2 = h$	$h_1 = 0.2h$ $h_2 = 1.8h$	$h_1 = h_2 = h$	$h_1 = 0.2h$ $h_2 = 1.8h$
11	3.835521 (13.0005%)	4.117346 (21.3035%)	3.427536 (0.9806%)	3.428572 (1.0112%)
21	3.609545 (6.3429%)	3.747731 (10.4141%)	3.402725 (0.2497%)	3.403911 (0.2846%)
41	3.500575 (3.1325%)	3.568789 (5.1422%)	3.396381 (0.0628%)	3.396773 (0.0743%)
81	3.447084 (1.5565%)	3.480947 (2.5542%)	3.394784 (0.0157%)	3.394893 (0.0189%)
161	3.420585 (0.7758%)	3.437453 (1.2728%)	3.394384 (0.0039%)	3.394413 (0.0048%)

ferences varied from about 1% at low rotation speeds to 0 at $\omega / 2\pi \approx 115\,\mathrm{s}^{-1}$. At $\omega / 2\pi > 115\,\mathrm{s}^{-1}$, displacements of a cylinder with square fibers became larger than those with round fibers. In this case, significant differences reached only near the limiting rotation speed, which was practically the same for both cylinders.

An analytical solution by finite formulas of the original problem, and even for the limiting one with fibers made of a binder material that remains geometrically and physically nonlinear is not possible. To make sure of the reliability of realization of the limiting problem, along with it, the corresponding problem was solved according to the relations of the linear elasticity theory, — in a two-dimensional formulation with discretizations in the case of cylinders with fibers of square and circular cross sections. The displacements based on the sampling data coincided with each other and with the results of the exact analytical solution according to the finite formulas given in [26] up to the fifth significant digit inclusive. The results of solving the limiting problem in a nonlinear formulation demonstrated a fast convergence of the corresponding linear problem to the exact solution with decreasing rotational speed of a cylindrical body.

We also solved the problem for a thick-walled cylinder made of an isotropic material in nonlinear and linear one-dimensional formulations, whose results were compared with the analytical solution. The internal and external radii of the cylinder $a = 100$ mm and $b = 200$ mm, respectively. The cylinder material was the same as the binder in fiber-reinforced cylinders, and boundary conditions were similar. Numerical solutions were carried out on the basis of nodal points with a uniform and nonuniform arrangement along the radial coordinate (Fig. 9). The uneven arrangement of points was obtained

TABLE 3. Displacements of the Inner (Numerator) and Outer (Denominator) Surfaces of an Isotropic Cylinder ($a = 100$ mm, $b = 200$ mm) under the Influence of Rotation from the Solutions of the Boundary-Value Problem in Nonlinear and Linear Formulations and the Exact Solution of the Linear Problem

$\dfrac{\omega}{2\pi}$, s^{-1}	Nonlinear elasticity theory	Linear elasticity theory	Exact solution by the linear elasticity theory
2.5	$\dfrac{0.21274}{0.12161}$	$\dfrac{0.21215}{0.12123}$	$\dfrac{0.21214}{0.12122}$
5	$\dfrac{0.85807}{0.49109}$	$\dfrac{0.84860}{0.48492}$	$\dfrac{0.84856}{0.48489}$
10	$\dfrac{3.55213}{2.04292}$	$\dfrac{3.39438}{1.93967}$	$\dfrac{3.39425}{1.93957}$
20	$\dfrac{16.6025}{9.78121}$	$\dfrac{13.5775}{7.75868}$	$\dfrac{13.5770}{7.75829}$
30	$\dfrac{54.3049}{34.2008}$	$\dfrac{30.5495}{17.4570}$	$\dfrac{30.5483}{17.4562}$
35	$\dfrac{118.090}{81.4048}$	$\dfrac{41.5812}{23.7610}$	$\dfrac{41.5796}{23.7598}$
37	$\dfrac{220.022}{166.709}$	$\dfrac{46.4691}{26.5541}$	$\dfrac{46.4673}{26.5527}$

on the basis of a uniform displacement of points with even numbers relative to points with odd numbers, but with an unchanged the position of the latter. In the case of a second-order approximation (by three points), the calculation results practically did not depend on the relative position of the points, although the adjacent gaps between them could differ tens of times. At a further approach of the even points to the odd ones, the calculation stability was practically stepwise lost. Calculation results were obtained with a high accuracy at a relatively small number of nodal points.

A qualitatively different picture was found at a linear (by two points) at a uniform arrangement of nodal points, their number of an order of magnitude greater was required than in the case of the second-order approximation to achieve the same 1% error compared with exact results. When the positions of even points approach the odd ones, the stability of the calculation was preserved. The accuracy of the results of solving the problem decreased with decreasing distance between the approaching points.

Table 2 shows the radial displacement u_a of inner surface of the cylinder found at $\omega = 2\pi \cdot 10\,\mathrm{s}^{-1}$ from the solution of the boundary-value problem in a linear formulation. Approximations of the first and second orders were performed using a uniform arrangement of nodal points, $h_1 = h_2 = h$, and an uneven one when the adjacent intervals between the points were equal, $h_1 = 0.2h$ and $h_2 = 1.8h$. The difference between displacements from the numerical solution of the problem and displacement $u_a = 3.394251$, found by the exact solution formulas (the exact value of the outer surface displacement $u_b = 1.939572$) are shown. The changes in these differences with transition from one density of nodes to another quite clearly reflects the linear and quadratic convergences for the approximations used. The same accuracy of results was achieved for all values of the deformed state at all nodal points along the thickness of the cylinder wall.

Table 3 shows the radial displacements of inner and outer surfaces of the cylinder at different speeds of rotation found from the numerical solution of the boundary-value problem in nonlinear and linear formulations and the exact solution of the linear problem. Numerical solutions of the problem were carried out on the basis of a second-order approximation with a total number of sampling points $N = 161$. These data were presented for the arrangement of nodal points uniformly across the cylinder thickness, since the unevenness of the arrangement, especially with such a great number of them, practically had no effect. For large displacements, the numerical and analytical solutions of the linear problem were, of course, formal. From the solution of the nonlinear problem, the angular speed of rotation $\omega = 2\pi \cdot 37\,\mathrm{s}^{-1}$ was found close

to the limiting one, at which, in the absence of destruction, the configuration of the cylinder developed indefinitely. The results presented reflect the nature of convergence of the results of nonlinear solution of the problem compared with that in the linear one with decreasing speed of cylinder rotation.

Conclusion

The implicit finite differences method (IFDM) has been described. It is convenient to use in the case of an irregular arrangement of nodal points of a discrete body scheme in the problem of its deformation. This method can be used to study bodies with irregular configurations and irregular shapes of inclusions. This method makes it possible, based on the formulation of the boundary-value problem in displacements and stresses as independent basic quantities of the resolving system of equations, to determine stresses with a higher accuracy than the FEM in the form of the displacement method. We also point to a simpler implementation of the problematics, especially nonlinear ones, using the IFDM than in the case of the FEM based on a variational formulation using piecewise approximation of the sought-for functions. (Of course, if the problem is solved on the basis of an extremal formulation that presupposes direct optimization of the state functional, the finite-element approximation, an alternative according to the finite-difference scheme does not exist.)

Obtaining high-precision results based on the approach described was demonstrated by examples of rotating cylinders with fibers of circular and square cross sections. The behavior of cylinders with different fibers with the same filling differed noticeably only when the rotation speed approaches the limiting one, when the unequal distribution of fiber material in the cylinders was affected by different shapes of their cross sections. The reliability of the computer implementation was directly confirmed by the results of solving the problem for a cylinder reinforced with square fibers using the finite-difference method with determinate coefficients.

The possibilities of the approach were also illustrated by the results of solving the boundary-value problem in nonlinear and linear formulations for a rotating thick-walled cylinder made of an isotropic material. The boundary-value problem was solved using the first- and second-order approximation for the basic quantities using a uniform and nonuniform distributions of nodal points over the cylinder wall. The results of numerical realizations were compared with results of the analytical solution of the linear problem by finite formulas. A high accuracy of solution of the problem was revealed in the case of quadratic approximation with a rather loose mesh of nodal points, which practically did not depend on their nonuniform arrangement.

REFERENCES

1. A. K. Malmeister, V. P. Tamuzh, and G. A. Teters, Resistance of Polymer and Composite Materials [in Russian], Riga: Zinatne (1980).
2. E. I. Grigolyuk and G. M. Kulikov, Multilayer Reinforced Shells. Calculation of Pneumatic Tires [in Russian], M.: Mashinostroenie (1988).
3. V. V. Kirichevsky, Method of Finite Elements in Mechanics of Elastomers [in Russian], K.: Nauk. Dumka (2002).
4. K. F. Chernykh, Nonlinear Elasticity Theory in Machine-Building Calculations [in Russian], L.: Mashinostroenie, (1986).
5. G. A. Holzapfel, T. C. Gasser, and R. W. Ogden, "A new constitutive framework for arterial wall mechanics and a comparative study of material models," J. Elasticity, **61**, 1-48 (2000).
6. G. A. Holzapfel, T. C. Gasser, and M. Stadler, "A structural model for the viscoelastic behavior of arterial walls: Continuum formulation and finite element analysis," Eur. J. Mech. A / Solids, **21**, 441-463 (2002).
7. W. J. Poole, J. D. Embury, S. MacEwen, and U. Kocks, "Large strain deformation of a copper-tungsten composite system. 1. Strain distribution," Philosoph. Mag. A, **69**, No. 4, 645-665 (1994).
8. P. D. Nicolaou, H. R. Piehler, and S. Saigal, "Process parameter selection for the consolidation of continuous fiber reinforced composites using finite element simulations," Int. J. Mech. Sci., **37**, No. 7, 669-690 (1995).

9. M. Gotoh and A. B. M. Idris, "Finite-element simulation of deformation of fiber-reinforced materials in the plastic range. Model proposition and tensile behaviors," JSME Int. J. Ser. A. Mech. Mater. Eng., **40**, No. 2, 149-157 (1997).

10. L. Banks-Sills and V. Leiderman, "Macro-mechanical material model for fiber reinforced metal matrix composites," Composites: Part B., **30**, Jan., 443-452 (1999).

11. Yu. V. Kokhanenko, "Numerical study of edge effects in layered composites under uniaxial loading," Prikl. Mekh., **46**, No. 5, 29-45 (2010).

12. S. Sockalingam, J. W. Gillespie, and M. Keefe, "On the transverse compression response of Kevlar KM2 using fiber-level finite element model," Int. J. Solids Struct., **51**, Jun., 2504-2517 (2014).

13. V. M. Akhundov, "Forming of a toroidal body with a cross-ply arrangement of fibers on the basis of a two-level carcas theory," Mech. Compos. Mater., **53**, No. 2, 253-266 (2017).

14. V. M. Akhundov, "A method for calculating the near-surface effect in piecewise-homogeneous bodies at large deformations on the basis of a two-level approach. materials," Mech. Compos. Mater., **56**, No. 2, 169-184 (2020).

15. F. L. Chernousko and V. P. Banichuk, Variational Problems of Mechanics and Control [in Russian], M.: Nauka (1973).

16. O. K. Zenkevich and K. Morgan, Finite Elements and Approximation [Russian translation], M.: Mir (1986).

17. V. M. Akhundov and M. M. Kostrova, "Nonlinear deformation of a piecewise-homogeneous cylinder under the influence of rotation," Mech. Compos. Mater., **54**, No. 2, 231-242 (2018).

18. V. M. Akhundov, I. Yu. Naumova, and A. A. Zabrodskaya, "Elastoreinforced pipe from three layers with ring fibers under the influence of internal pressure," Visnik Zaporiz. Nats. Univ., No. 1, 4-13 (2019).

19. T. Shup, Solving Engineering Problems on a Computer [Russian translation], M.: Mir, (1982).

20. N. S. Bakhvalov, N. P. Zhidkov, and G. M. Kobelkov, Numerical Methods [in Russian], M.: Nauka (1987).

21. J. Ortega and V. Reinboldt, Iterative Methods for Solving Nonlinear Systems of Equations with Many Unknowns [Russian translation], M.: Mir (1975).

22. F. P. Vasiliev, Optimization Methods [in Russian], M.: Izd "Faktorial Press," (2002).

23. A. I. Lurie, Nonlinear Elasticity Theory [in Russian], M.: Nauka (1980).

24. V. M. Akhundov, "Analysis of elastomeric composites based on fiber systems. 1. Development of a method for calculating composite materials," Mech. Compos. Mater., **34**, No. 6, 515-524 (1998).

25. V. Z. Parton and P. I. Perlin, Methods of mathematical elasticity theory [in Russian], M.: Nauka (1981).

26. S. D. Ponomarev, Strength Calculations in Mechanical Engineering," S. D. Ponomarev et al., **3**, 32-41, Mashgiz, Moscow (1959).